PCCP

RSC Publishing

COMMUNICATION

View Article Online
View Journal | View Issue

Influence of catalyst choices on transport behaviors of InAs NWs for high-performance nanoscale transistors†

Cite this: *Phys. Chem. Chem. Phys.*, 2013, **15**, 2654

Received 26th November 2012,
Accepted 20th December 2012

DOI: 10.1039/c2cp44213b

www.rsc.org/pccp

Szu-Ying Chen,[a] Chiu-Yen Wang,[a] Alexandra C. Ford,[b] Jen-Chun Chou,[a] Yi-Chung Wang,[a] Feng-Yun Wang,[c] Johnny C. Ho,[c] Hsiang-Chen Wang,[d] Ali Javey,[b] Jon-Yiew Gan,[a] Lih-Juann Chen*[a] and Yu-Lun Chueh*[a]

The influence of the catalyst materials on the electron transport behaviors of InAs nanowires (NWs) grown by a conventional vapor transport technique is investigated. Utilizing the NW field-effect transistor (FET) device structure, ~20% and ~80% of Au-catalyzed InAs NWs exhibit strong and weak gate dependence characteristics, respectively. In contrast, ~98% of Ni-catalyzed InAs NWs demonstrate a uniform n-type behavior with strong gate dependence, resulting in an average OFF current of $\sim 10^{-10}$ A and a high I_{ON}/I_{OFF} ratio of $>10^4$. The non-uniform device performance of Au-catalyzed NWs is mainly attributed to the non-stoichiometric composition of the NWs grown from a different segregation behavior as compared to the Ni case, which is further supported by the *in situ* TEM studies. These distinct electrical characteristics associated with different catalysts were further investigated by the first principles calculation. Moreover, top-gated and large-scale parallel-array FETs were fabricated with Ni-catalyzed NWs by contact printing and channel metallization techniques, which yield excellent electrical performance. The results shed light on the direct correlation of the device performance with the catalyst choice.

Introduction

In recent years, significant progress has been achieved in the assembly of semiconductor nanowires (NWs) for the large-area device integration while the essential demands toward commercialization of such NW-based devices still highly rely on the accomplishment of uniformly reliable and controllable NW physical properties. The NW growths, including vapor–liquid–solid (VLS) or vapor–solid–solid (VSS), were typically utilized to realize a precise control of the growth position and morphology. However, *in situ* doping of impurities through the metal catalyst into nanowires during the NW growth may alter intrinsic electrical properties of NWs. In particular, InAs NWs have been widely explored as the channel material for high performance transistors owing to their high electron mobility ($\sim 10\,000$ cm^2 V^{-1} s^{-1}) and ability to readily form a near-ohmic contact with metal electrodes due to a small band gap and an intrinsic surface charge behavior.[1,2] The synthesis of InAs NWs has been achieved by a metal–organic chemical-vapor deposition (MOCVD) method, with which Au nanoparticles were commonly used as the growth catalyst. The growth has been carefully controlled with different V/III ratios between As and In not only to achieve the lowest density of crystal defects such as As-antisites and As interstitials but also to reduce the tapered morphology owing to an overcoating *via* an uncontrolled adatom diffusion.[3–5]

In addition to MOCVD, a simple way utilizing a conventional furnace to grow InAs NWs *via* InAs powders as the growth precursor has also been demonstrated successfully regardless of the control of the V/III ratio.[6] Furthermore, the electrical transport of NWs has been evidently demonstrated as the diameter of InAs NWs <30 nm grown by the same approach.[7] However, it is still unclear how the metal catalysts could influence the intrinsic electrical transport properties of III–V nanowires as well as the nanowire morphology. In this regard, we found a substantial influence on the morphology and electron transport behaviors of InAs NWs with different metal catalysts, which would provide valuable insights into controlling and achieving uniform physical properties of NWs for large-scale high-performance device applications.

[a] *Department of Materials Science and Engineering, National Tsing Hua University, Hsinchu, 30013, Taiwan, R.O.C. E-mail: ljchen@mx.nthu.edu.tw, ylchueh@mx.nthu.edu.tw*
[b] *Department of Electrical Engineering and Computer Sciences, University of California at Berkeley, Berkeley, CA 94720, USA*
[c] *Department of Physics and Materials Science, City University of Hong Kong, Tat Chee Avenue Kowloon, Hong Kong SAR, China*
[d] *Graduate Institute of Opto-Mechatronics, National Chung Cheng University 168, University Rd., Min-Hsiung, Chia-Yi 62102, Taiwan*

† Electronic supplementary information (ESI) available: Contrast profile along the axis of Au-catalyzed InAs NWs; I_{DS}–V_{DS} curves for four more top gate transistor devices. SEM and optical images of Ni-catalyzed InAs NW array devices and the corresponding I_{DS}–V_{GS} curves at a channel width of 36 μm with a channel length of ~1.5 μm after the metallization process. See DOI: 10.1039/c2cp44213b

Results and discussion

NWs were grown by using the previously reported vapor transport technique.[6] Briefly, 1.5 nm-thick Ni or Au thin films were deposited by e-beam evaporation on Si/SiO_2 substrates. Subsequently, the samples were annealed at 800 °C to form the Ni or Au nanoparticles (NPs) with average diameters of ~30–50 nm. The growth furnace simply consists of two independently controlled temperature zones, namely the high temperature zone at 700–800 °C for the vaporization of InAs solid source and the low temperature zone at 400–550 °C for the growth of InAs NWs with 200 sccm hydrogen (H_2) gas as the carrier gas. The pressure was maintained at 1–0.8 Torr. The corresponding SEM images of Ni-catalyzed and Au-catalyzed InAs NWs are shown in Fig. 1(a) and (b), respectively, grown with the identical conditions of pressure, temperature, and time being 0.8 Torr, 520 °C, and 30 min, respectively. Clearly, the InAs NWs grown from Ni NPs as the catalyst have a long and straight morphology with an average length >15 μm whereas NWs with a shorter length of <6 μm and a distinct tapered morphology are observed using Au NPs as the catalysts. Insets show the magnified SEM images of tip regions for the two cases, for which catalysts at both samples are clearly seen, confirming a catalytic growth mechanism, namely, VLS/VSS.[8,9] The crystal phase formation was also investigated by grazing incidence X-ray diffraction (GIXRD) as shown in Fig. 1(c) and (d) for Ni-catalyzed and Au-catalyzed InAs NWs, respectively. Peaks at 240, 420, and 500, corresponding to (111), (220), and (311) were indexed for both spectra, which match the phase of InAs. Extra peaks at (211) and (311) in Fig. 1(d) could be ascribed to a phase of Au_7In_3, which is originated from a solid reaction between In and Au catalyst during the NW growth.[10]

Fig. 2(a) and (b) show the transmission electron microscopy (TEM) images of representative Ni- and Au-catalyzed InAs NWs, respectively. Obviously, the tapered morphology is observed for the Au-catalyzed InAs NW, which is most likely induced by an overcoating *via* the uncontrolled InAs adatom diffusion during the growth while no overcoating behavior is observed for the Ni-catalyzed InAs NWs. Fig. 2(c) and (d) show the high resolution TEM images taken from rectangular areas in Fig. 2(a) and (b), respectively, for which (111) planes were indexed with a plane spacing of 0.35 nm. Insets show the corresponding selected area diffraction patterns (SAD) processed with a fast Fourier transform (FFT) technique. As a result, InAs NWs exhibit a single crystalline feature with the growth direction along the [110] direction regardless of different catalysts. In addition, elemental profiles of the tip regions are shown in Fig. 2(e) and (f). Interestingly, for Ni-catalyzed InAs NWs, the catalyst consists of Ni, In, and As with compositions of ~58 at%, ~22 at%, and ~20 at%, respectively, yielding a chemical configuration of Ni_2InAs while for Au-catalyzed InAs NWs, the catalyst only consists of Au and In with compositions of ~72 at% and ~28 at%, which agree with the phase of Au_7In_3 as detected by XRD. In addition to the catalyst, we found that compositions of InAs NWs grown from the Ni- and the Au-NPs are quite different. The chemical compositions of Ni-catalyzed InAs NWs are uniform with ~51 at% In and ~49 at% As while the compositions of ~61 at% In and ~39 at% As, namely In-rich InAs NWs, are typically found for Au-catalyzed InAs NWs. The NWs with different compositions of In and As and the tapered morphology are most likely to be highly influenced by different segregation behaviors due to the different catalysts with Au_7In_3 and Ni_2InAs phases and will be discussed in detail later.

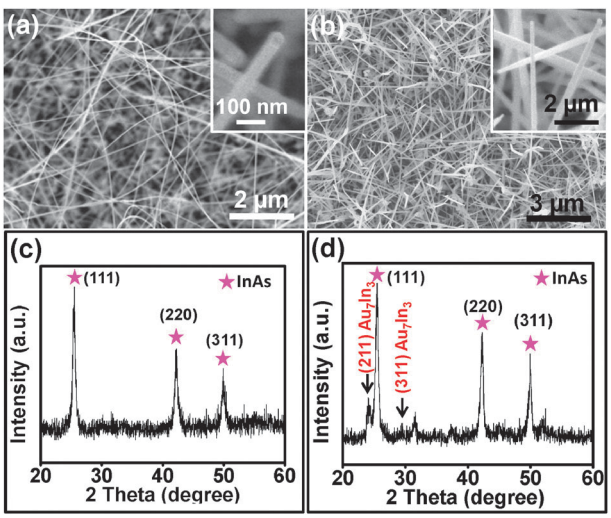

Fig. 1 Scanning electron microscopy (SEM) images of (a) Ni-catalyzed InAs NWs and (b) Au-catalyzed InAs NWs. (c) and (d) show the corresponding grazing incidence X-ray diffraction (GIXRD) spectra for InAs NWs grown from Ni and Au catalysts, respectively.

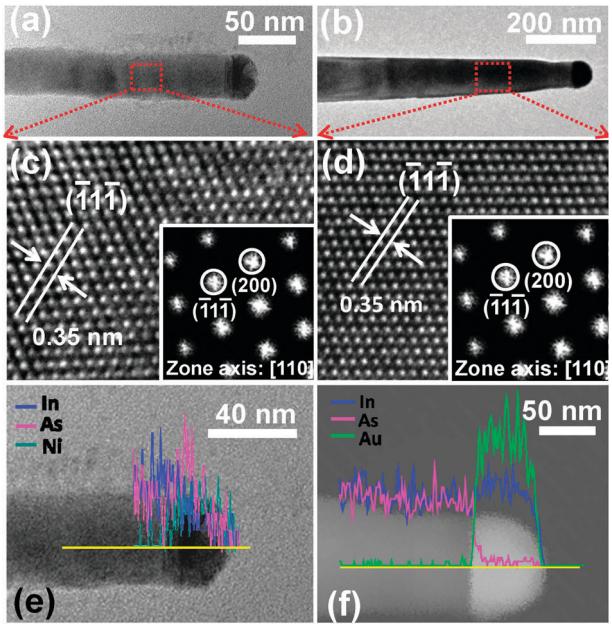

Fig. 2 TEM images of (a) a typical Ni-catalyzed InAs NW and (b) Au-catalyzed InAs NW. The corresponding high-resolution TEM images are shown in (c) and (d) for Ni-catalyzed and Au-catalyzed InAs NWs, respectively. The inset shows the corresponding diffraction patterns with the identical zone axis of [110] zone converted by fast-Fourier transform (FFT). (e) and (f) show the elemental profiles for Ni-catalyzed and Au-catalyzed InAs NWs, for which, the colors, light green, dark green, blue, and pink represent Au, Ni, In, and As, respectively.

In order to characterize how the catalytic materials influence the electrical properties of InAs NWs, field-effect transistors (FETs) were fabricated and characterized. The grown NWs were drop-cast on Si/SiO_2 substrates (50 nm, thermal oxide as the gate dielectric layer and heavily B doped Si as the global back gate), followed by the photolithography patterning of S/D electrodes *via* thermal evaporation of Ni (50 nm-thick) and lift-off processes. A 0.5 wt% HF treatment of ~5 s was applied to remove the native oxide prior to the metallization. The representative I_{DS}–V_{GS} curves at V_{DS} = 0.1, 0.3, and 0.5 V for Ni- and Au-catalyzed InAs NWs are shown in Fig. 3(a) and (b), respectively. Notably, the Ni-catalyzed InAs NW with the diameter of ~35 nm device exhibits clear n-type switching characteristics with strong gate modulation of conductance, yielding an OFF current of ~0.1 nA and an I_{ON}/I_{OFF} ratio of ~10^4 at V_{DS} = 0.1 V and V_{GS} = −2 V while the Au-catalyzed InAs NW with the diameter of ~100 nm device shows a near metallic behavior with weak gate dependence, resulting in a much higher OFF current of ~10 μA and a smaller I_{ON}/I_{OFF} ratio of ~2 at V_{DS} = 0.1 V and V_{GS} = −4 V. To gain a better insight on the electrical uniformity of both Ni- and Au-catalyzed InAs NWs, more than 100 devices from Ni- and Au-catalyzed InAs NWs were fabricated. The statistical data of the I_{ON}/I_{OFF} ratios and the corresponding smallest OFF currents are shown in Fig. 3(c) and (d), respectively. Notably, utilizing Au as the growth catalyst, ~80% and ~20% of grown InAs NWs exhibit weak and strong gate modulation behaviors, respectively, for which a wide range of I_{ON}/I_{OFF} ratios (~1 to ~10^4) and OFF currents (~10^{-5} to ~10^{-10} A) were observed. On the other hand, with the Ni catalysts, ~98% of grown InAs NWs exhibit strong gate modulation with the relatively uniform I_{ON}/I_{OFF} ratios (~10^3 to ~10^5) and low OFF currents (~10^{-8} to ~10^{-11} A).

To shed light on how the catalyst can influence the growth of InAs NWs, *in situ* TEM observation of the solid reaction between the metal catalyst and InAs is imperative. Due to the difficulty in direct observation of InAs NW growth inside the TEM, we, therefore, chose a simple way by directly observing solid state reactions between Au or Ni films on InAs crystals. The TEM samples of Au/InAs and Ni/InAs samples were prepared *via* the focus ion beam (FIB) method on the TEM grids, followed by *in situ* heating of the samples inside a TEM with a heating stage (Gatan 652 double tilt heating holder) at a pressure below 10^{-6} Torr.[11,12] Heater temperature was elevated to 300 °C with a step of 50 °C. To completely observe the solid state reaction, each annealing temperature was maintained for 20 min. The compositions were *in situ* monitored by energy dispersive X-ray spectroscopy (EDS) measurements. Fig. 4 shows the *in situ* TEM images of the solid state reactions between InAs and Ni or Au films in real-time. As depicted in Fig. 4(a1)–(a3) with annealing temperatures from 25 to 250 °C for the Au case, In and As atoms are both dissolved into Au thin films with atomic compositions of Au, In, and As being ~79 at%, ~17 at%, and ~4 at% at 150 °C and then were changed to ~57 at%, ~27 at%, and ~16 at% at 250 °C, respectively, as listed in Table 1. Interestingly, increasing concentrations of As atoms in the $AuInAs_x$ metastable alloy at elevated temperature could be found. These results could infer that As atoms are most likely involved in the nanowire growth from Au catalysts. Once the

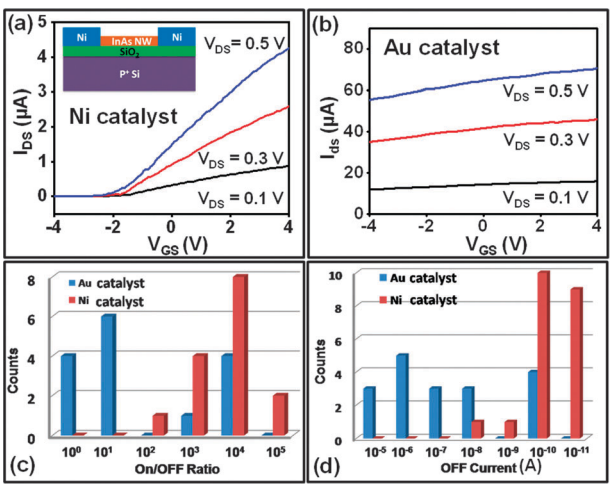

Fig. 3 I_{DS}–V_{GS} curves of InAs NWs FETs at V_{DS} = 0.1, 0.3 and 0.5 V grown from (a) Ni and (b) Au as catalysts. Statistical results of (c) I_{ON}/I_{OFF} ratios and (d) OFF currents extracted from 100 devices based on Ni-catalyzed and Au-catalyzed InAs NWs, respectively.

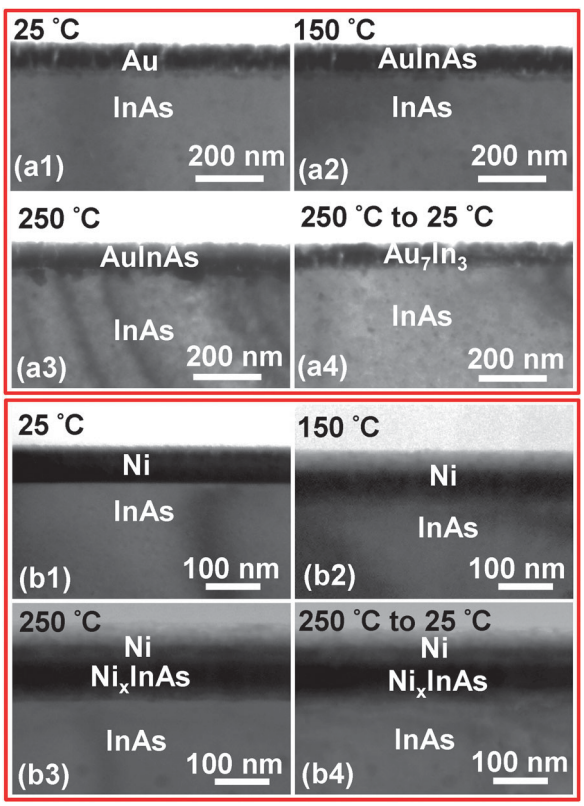

Fig. 4 *In situ* TEM images of the solid state reaction between Au and InAs substrate at elevated annealing temperatures of (a1) 25 °C, (a2) 150 °C, and (a3) 250 °C. (a4) shows the TEM image of the sample after cooling down to 25 °C. *In situ* TEM images of the solid state reaction between Au and InAs substrate at elevated annealing temperatures of (b1) 25 °C, (b2) 150 °C, and (b3) 250 °C. (b4) shows the TEM image of the sample after cooling down to 25 °C.

Table 1 *In situ* EDS results of solid state reactions between Au and InAs at different annealing temperatures

	25 °C	150 °C	250 °C	25 °C
Au (at%)	100	79	57	69
In (at%)	0	17	27	31
As (at%)	0	4	16	0

temperature was cooled down to room temperature, all the As atoms are excluded out of the $AuInAs_x$ metastable alloy, resulting in a Au_7In_3 phase, which appears with island structures as shown in Fig. 4(a4). In contrast with the Au case, as shown in Fig. 4(b1)–(b3), no obvious solid state reaction is observed under 100 °C for the Ni case while an internal diffusion layer formed by a solid state reaction between Ni and InAs was found as the annealing temperature is increased to over 150 °C with the atomic compositions of Ni, In, and As being ~51, ~25, and ~24 at%, respectively. The compositions remained the same as the annealing temperature is increased to 250 °C, indicating the formation of a stable phase, namely Ni_2InAs.[13] In addition, the chemical composition is unchanged after the sample is cooled down to room temperature, which is consistent with that of the catalyst for Ni-catalyzed InAs NWs as confirmed by EDS.

Accordingly, the possible growth mechanism for nanowires with these two kinds of metal catalysts could be investigated as shown in Fig. 5. Clearly, the catalytic seeds are observed at the tips of Au- and Ni-catalyzed NWs, which could be inferred to possess a distinct characteristic of the catalytic VLS or VSS growth mechanism. As previously mentioned for the growth of InAs NWs with Au catalysts, As atoms would probably react with In segregated from the Au_7In_3 catalyst at the catalyst–NW interface rather than dissolving in/or alloying with the Au_7In_3 catalyst due to their relatively low solubility in Au.[14] However, this assumption does not exactly match our *in situ* TEM observation as we have found that As atoms can indeed be dissolved into the

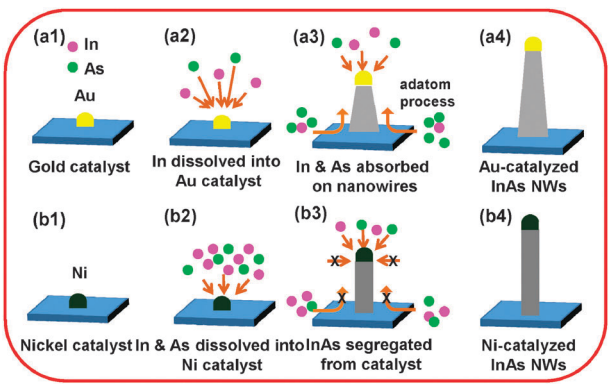

Fig. 5 Schematics of growth mechanisms for InAs NWs from Au and Ni as the catalyst. (a1) Formation of Au NPs from Au film after annealing; (a2) solid state reaction of Au NPs with In and As into metastable $AuInAs_x$; (a3)–(a4) axial growth of InAs NWs segregated from the $AuInAs_x$ supersaturated catalyst. The adatom process will be dominated to result in tapered morphology once $l > \lambda_{NW}$. (b1) Formation of Ni NPs from Ni film after thermal annealing; (b2) formation of the Ni_xInAs catalyst; (b3)–(b4) axial growth of InAs NW segregated from the catalyst without the occurrence of overcoating.

catalyst, resulting in the formation of a metastable $AuInAs_x$ alloy during nanowire growth (Fig. 5(a1)–(a2)). In other words, the segregation of In and As atoms from the metastable $AuInAs_x$ catalyst would partially contribute to the growth of InAs NWs with a growth rate of ~3 nm s^{-1}, extracted from the SEM image at different growth times. In addition, the spherical shape of observed catalytic seeds after nanowire growth provides evidence of the molten catalyst in its liquid state, suggesting that Au-catalyzed InAs growth is carried out *via* the VLS mechanism. Simultaneously, an adatom diffusion process, namely noncatalytic radial deposition of InAs NWs, occurs, leading to a tapered morphology as shown in Fig. 5(a2)–(a3). It was reported that when the NW length (l) is shorter than the surface diffusion length on NW sidewalls (λNW), the overcoating due to In adatoms impinging on NW sidewalls continuously increases with time, leading to the superlinear growth rate, for which the growth of NW length exponentially increases with the time, namely VLS without any overcoating.[15] After $l > \lambda$NW for the longer growth time, the growth rate of NWs is turned from the superlinear into the linear modes so that the surface diffusion *via* the overcoating occurs.[15] The effect of this surface diffusion (overcoating) is manifested *via* the changes of the NW diameter during the growth. By drawing a contrast profile along the axis of NWs, we are able to extract the λNW ~70 nm as shown in Fig. S1(a) (ESI†). Compared with Au-catalyzed InAs NWs, the growth of NWs from Ni NPs shows a long and straight morphology with a growth rate of ~9 nm s^{-1}, which is much faster than that of Au-catalyzed InAs NWs (~3 nm s^{-1}). The corresponding schematics illustrating the growth of Ni-catalyzed InAs NW is shown in Fig. 5(b1)–(b4). Initially, the Ni catalyst can alloy with In and As atoms to form the Ni_xInAs alloy catalyst with high concentrations of In (~24 at%) and As (~25 at%) confirmed by EDS (Fig. 5(b1)–(b2)). Subsequently, the axial growth of NWs resulted from the segregation of In and As atoms out of the Ni_xInAs catalyst can be achieved once the Ni_xInAs alloy catalyst reaches a supersaturation condition, which is the typical catalytic growth mechanism (Fig. 5(b3)–(b4)). It is worth noting that straight Ni-catalyzed InAs NWs indicate no lateral growth of NWs, ruling out the adatom diffusion, namely overcoating on the surface of InAs NWs (Fig. S1b, ESI†). The absence of the InAs overcoating is mainly attributed to the fast growth rate suppressing the lateral growth. It has been observed that at the identical growth temperature, the growth rate from VLS is normally one order of magnitude faster than that of VSS for the same NW while the observed results are not suitable in our case due to different chemical compositions found in the catalysts for Ni- and Au-catalyzed InAs NWs.[16] The slow growth of Au-catalyzed InAs NWs is because excess In atoms segregated out of the catalyst need more time to bond with As atoms coming from the adatom diffusion, which also triggers the lateral growth. However, the exclusive supply of In and As atoms from the Ni_xInAs catalyst could result in the fast growth rate without the lateral growth, thereby yielding a less defective and stoichiometric NW.

In addition, the growth of III–V nanowires is known to be a mass-transport limited process where the smaller diameter nanowires will grow much faster and the growth rate shows

an exponential increase as the diameter of NW < ~60 nm.[17] However, the growth rate does not change significantly when the diameter > ~60 nm. In the present research, the diameters of Au-catalyzed InAs NWs are typically over 60 nm, exhibiting the less dependence with diameter variation while a clear growth rate dependence with diameter variation can be observed for the Ni-catalyzed InAs NWs. The smaller the diameter of the Ni catalyst, the faster the growth rate of Ni-catalyzed InAs NWs. This is why the Ni-catalyzed InAs NWs have a much faster growth rate than that of Au-catalyzed InAs.

Moreover, the lateral growth or sidewall overcoating may induce intrinsic defects such as In interstitials or As vacancies, resulting in the unstable and non-uniform electrical properties of grown NWs. To further understand the influence of these defects on electrical properties, the first principle calculation was performed to assess the corresponding density of states and their effects on NW transport *via* a density functional theory (DFT) using the CASTEP (Cambridge serial total Energy package) module. Based on the EDS results, Ni- and Au-catalyzed InAs NWs with the atomic ratios of In to As being 1 to 1 and 1 to 0.625 due to As vacancies were taken into account in the calculation, respectively (for detailed simulation processes, please see the ESI†). Consequently, typical partial density of states (PDOS) for both Ni- and Au-catalyzed InAs NWs were constructed as shown in Fig. 6(a) and (b). Notably, a distinct overlap of As-4p and In-5p from −3.5 to 0.3 eV with a band gap of ~0.35 eV could be obtained for InAs without As vacancies while a change of overlap in the energy level could be observed after rebuilding of As–In covalent bonds from In-5s, In-5p, As-4p, and a few As-4s to the unoccupied high energy levels across the Fermi level, resulting in n^+ type semiconducting or even metallic-like properties after the formation of As vacancies. In addition, segregation of Au clusters on the surface of the NW or in the NW from the Au catalyst *via* the VLS or VSS mechanism may be another issue of the unstable electrical transport properties.[18,19]

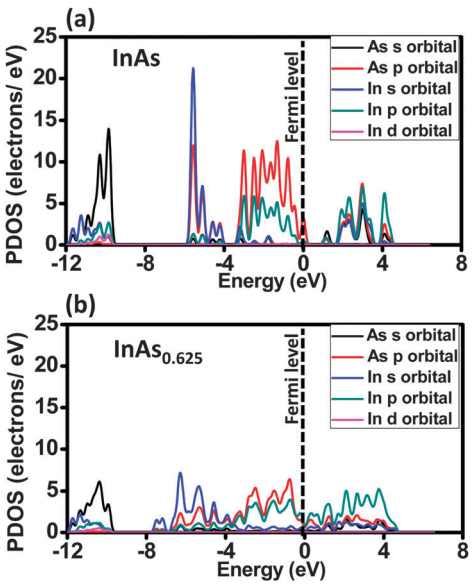

Fig. 6 Partial density of state (PDOS) of (a) In_8As_8 (pure InAs) and (b) In_8As_5 (with three intrinsic As vacancies).

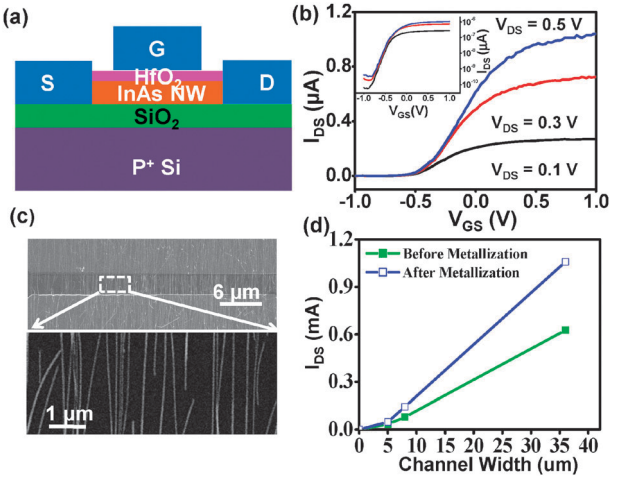

Fig. 7 (a) Schematic of the top gate device based on a Ni-catalyzed InAs NW. The corresponding top gate I_{DS}–V_{GS} curves. (c) Optical and SEM images of controlled channel length at a channel width of 36 μm after the metallization process. (d) The corresponding I_{DS} as the function of channel widths before and after the metallization.

In this case, the balanced stoichiometry of InAs NWs is important to achieve uniform and high-performance NW electronic device arrays. To shed light on the performance limits of Ni-catalyzed InAs NWs, top gate NW field effect transistors were fabricated with a 8 nm thick HfO_2 dielectric layer deposited by an atomic layer deposition system (ALD) as depicted in the device schematic (Fig. 7a). Fig. 7(b) shows the I_{DS}–V_{GS} results at V_{DS} = 0.1, 0.3 and 0.5 V, respectively, and the inset illustrates the corresponding logarithm-scale plot. Specifically, the device exhibits an impressive OFF current (~10^{-10}A) at V_{DS} = 0.1 V and an excellent I_{ON}/I_{OFF} ratio (~10^6) with the sub-threshold swings of ~130–160 mV dec^{-1} (more device measurements are shown in Fig. S2, ESI†). The very stable and electrically uniform InAs NWs grown from the Ni catalyst are suitable for large-scale array devices *via* a contact printing technique where the channel width of InAs NW arrays can be controlled with a nanowire density of ~5 NWs μm^{-1}.[13,20] A linear behavior of ON current with the increase of the channel width could be obtained.[21] The ON current could be further increased through the reduction of the channel length by the metallization process *via* formation of the metallic nanoelectrode, Ni_xInAs, as shown in Fig. 7(c) (~3 μm and ~1.5 μm before and after metallization, respectively).[13] The corresponding ON current as the function of channel widths before and after metallization is shown in Fig. 7(d) where the channel widths were changed from 5–36 μm with the fixed channel lengths (~3 μm and ~1.5 μm for before and after metallization, respectively). Obviously, ON-current of nanowire arrays increases linearly with the increasing channel width, yielding a slope of 19 μA μm^{-1} while the slope can be increased to 32 μA μm^{-1} after the reduction of channel length to ~1.5 μm *via* the metallization process. As a result, the highest ON-current of 1.1 mA at a channel width of 36 μm can be achieved (see ESI,† Fig. S3). InAs NW parallel array devices demonstrated the importance of the catalyst choice in controlling the transport properties for large-scale device applications.

Conclusions

In conclusion, the influence of catalyst choice and its catalytic effects on transport behaviors of InAs NWs have been investigated. The results indicated that the tapered morphology of InAs NWs grown with Au NPs as the catalyst yields the unstable and non-uniform electrical properties where ~80% and ~20% of InAs NWs exhibit strong and weak gate dependence characteristics, respectively. On the other hand, straight morphology is observed for InAs NWs grown with Ni NPs, in which ~98% of InAs NWs exhibit a very uniform n-type behavior with strong gate dependence, giving the impressive OFF current ($\sim 10^{-8}$–10^{-10} A) with the maximum $I_{ON}/I_{OFF} > 10^4$. The unstable and non-uniform electrical transport performance can be concluded from non-stoichiometric composition of InAs NWs due to the different segregation or NW growth schemes from the Au catalyst, which was supported by the *in situ* TEM observation. These distinct electrical characteristics associated with different catalysts were further investigated by the first principle calculation. Based on the electrically uniform and stable Ni-catalyzed InAs NWs, the excellent performance of top-gate InAs NW parallel array devices demonstrated the importance of the catalyst choice in controlling the transport properties for large-scale device applications.

Acknowledgements

The research was supported by the National Science Council through grant no. NSC 101-2218-E-007-009-MY3, NSC 101-2112-M-007-015-MY3, and NSC 98-2221-E-007-104-MY3, and by the General Research Fund of the Research Grants Council of Hong Kong SAR, China, under Project No. CityU 101111.

References

1 Y. L. Chueh, A. C. Ford, J. C. Ho, Z. A. Jacobson, Z. Fan, C. Y. Chen, L. J. Chou and A. Javey, *Nano Lett.*, 2008, **8**, 4528.
2 A. C. Ford, J. C. Ho, Y. L. Chueh, Y. C. Tseng, Z. Fan, J. Guo, J. Bokor and A. Javey, *Nano Lett.*, 2009, **9**, 360.
3 H. J. Joyce, Q. Gao, H. H. Tan, C. Jagadish, Y. Kim, Y. Guo and J. Zou, *Nano Lett.*, 2007, **7**.
4 H. J. Joyce, Q. Gao, H. H. Tan, C. Jagadish, Y. Kim, M. A. Fickenscher, S. Perera, T. B. Hoang, L. M. Smith, H. E. Jackson, J. M. Yarrison-Rice, X. Zhang and J. Zou, *Nano Lett.*, 2009, **9**, 695.
5 S. A. Dayeh, E. T. Yu and D. Wang, *Nano Lett.*, 2009, **9**, 1967.
6 C. F. Alexandra, J. C. Ho, Z. Fan, O. Ergen, V. Altoe, S. Aloni, H. Razavil and A. Javey, *Nano Res.*, 2008, **1**, 32.
7 A. C. Ford, S. B. Kumar, R. Kapadia, J. Guo and A. Javey, *Nano Lett.*, 2012, **12**, 1340.
8 Y. Wu and P. Yang, *J. Am. Chem. Soc.*, 2001, **123**, 3165.
9 Y. L. Chueh, Z. Fan, K. Takei, H. Ko, R. Kapadia, A. A. Rathore, N. Miller, K. Yu, M. Wu, E. E. Haller and A. Javey, *Nano Lett.*, 2010, **10**, 520.
10 T. Massalski, *Binary Alloys Phase Diagrams*, 1987.
11 Y. L. Chueh, C. N. Boswel, C. W. Yuan, S. J. Shin, K. Takei, J. C. Ho, H. Ko, Z. Fan, E. E. Haller, D. C. Chrzan and A. Javey, *Nano Lett.*, 2010, **10**, 393.
12 C. Y. Wang, N. W. Gong and L. J. Chen, *Adv. Mater.*, 2008, **20**, 4789.
13 Y. L. Chueh, A. C. Ford, J. C. Ho, Z. A. Jacobson, Z. Y. Fan, C. Y. Chen, L. J. Chou and A. Javey, *Nano Lett.*, 2008, **8**, 4528.
14 K. A. Dick, K. Deppert, T. Mårtensson, B. Mandl, L. Samuelson and W. Seifert, *Nano Lett.*, 2005, **5**, 761.
15 S. A. Dayeh, E. T. Yu and D. Wang, *Nano Lett.*, 2009, **9**, 1967.
16 S. Kodambaka, J. Tersoff, M. C. Reuter and F. M. Ross, *Science*, 2007, **316**, 729.
17 J. Johansson, C. P. T. Svensson, T. Mårtensson, L. Samuelson and W. Seifert, *J. Phys. Chem. B*, 2005, **109**, 13567.
18 H. D. Park, S. M. Prokes, M. E. Twigg, R. C. Cammarata and A. C. Gaillot, *Appl. Phys. Lett.*, 2006, **89**, 223125.
19 B. Mandl, J. Stangl, T. Mårtensson, A. Mikkelsen, J. Eriksson, L. S. Karlsson, G. Bauer, L. Samuelson and W. Seifert, *Nano Lett.*, 2006, **6**, 1817.
20 A. Javey, S. Nam, R. S. Friendman, H. Yan and C. M. Lieber, *Nano Lett.*, 2007, **7**, 773.
21 Z. Fan, J. C. Ho, Z. A. Jacobson, R. Yerushalmi, R. L. Alley, H. Razavi and A. Javey, *Nano Lett.*, 2008, **8**, 20–25.